J Mater Sci (2007) 42:5756–5765
DOI 10.1007/s10853-006-0671-x

Joint formation mechanism and strength in resistance microwelding of 316L stainless steel to Pt wire

Zheng Chen

Received: 14 December 2005 / Accepted: 14 July 2006 / Published online: 14 April 2007

Abstract Resistance microwelding of 316L stainless steel to Pt wire has been performed. The interfacial metallurgical phenomena, joint breaking force and fracture mode were investigated using scanning electron microscopy, energy-dispersive X-ray spectroscopy and tensile-shear testing. The results showed that a solid-state bonding was achieved at the interface when the welding current was low and/or the weld time was short, whereas a bonding with fusion of materials was observed at high welding current. Melting of the stainless steel was more significant than that of the Pt wire. The amount of melted materials and bonded area increased with increasing welding current and/or weld time. At a low welding current, e.g., 500 A, all the joints fractured at the interface and the joint breaking force rapidly increased when weld time prolonged from 2 ms to 10 ms owing to increased bonded area. At a medium welding current, e.g., 750 A, the joints demonstrated different fracture mode, e.g., at the interface, a mixed failure at the interface and in the Pt wire as well as completely within the Pt wire, as the weld time increased. On the other hand, at a high welding current, e.g., 1,000 A, the stainless steel was greatly melted and softened into which the Pt wire penetrated and all the joints fractured in the Pt wire. The joint breaking force first increased with increasing weld time and subsequently decreased after reaching a peak value. The effects of materials properties on dissimilar materials resistance welding process were also discussed.

Z. Chen (✉)
Department of Materials Science and Engineering, Jiangsu University of Science and Technology, Zhenjiang 212003, P.R. China
e-mail: chenz_31@yahoo.com.cn

Introduction

As a biocompatible metal, coupling with the good mechanical properties and outstanding corrosion resistance, AISI 316L stainless steel has been widely used for medical implants and medical devices and instruments [1–3]. As labor costs for medical manufacturing continue to rise, reductions in component manufacturing costs become ever more important for controlling overall costs. Many medical devices, especially instruments and implants, are produced from difficult-to-machine materials such as stainless steels. As a result, welding and joining processes as an alternative way could reduce the costs of fabricating components. On the other hand, manufacturing of medical devices in many instances requires joining a material to itself and to other dissimilar materials. For example, laser welding and diffusion bonding have been reported to join Co–Cr alloy [4], Ti–6Al–4V alloy-to-Pt [5], Ti–6Al–4V-to-AISI 316L [6] for the fabrication of metal frameworks and other devices in medical applications.

Resistance microwelding (RMW) is an important microjoining process used to fabricate electronic devices and components (such as batteries, capacitors and microsensors), in which thin metal sheets or wires (<0.2–0.5 mm in thickness or diameter), mostly nonferrous metals, are welded by resistance heating [7].

Compared with laser welding, RMW has advantages of low cost, simplicity and easy to carry out, and could find a wide applications in manufacturing of medical devices.

Based on the previous researches on RMW of Au-plated Ni sheet [8], Ni wire [9], Au-plated Ni wire [10] and Ni-plated steel [11, 12] as well as Cu and Al [13], the present work will apply RMW to join 316L stainless steel to Pt wire. The effects of welding current and weld time on welding process, interfacial bonding, joint strength and fracture of the joints will be investigated.

Experimental

Cold-worked Pt wires (diameter 0.36 mm) and 316L stainless steel block (6 mm × 3 mm × 3 mm) were used in this study. The Pt wire was bonded by resistance microwelding to the 316L stainless steel block. The composition of 316L stainless steel is listed in Table 1. Before welding, the Pt wire and the 316L SS block were ultrasonically cleaned in acetone for 10 min. The resistance microwelding system consisted of a MacGregor DC400P direct-current (DC) controller and a Unitek 80A/115 weld head (air activated). Flat-ended, round RWMA class II (Cu–Cr) electrodes, 3.2 mm in diameter, were used. All weld tests employed the same type of welding current program, in which current was increased from zero at a constant rate of 50 A/ms until the current setpoint value (500–1,000 A) was reached. Then current was maintained constant for a ''hold time'' (weld time) (2–100 ms) before being terminated. After RMW, the joint breaking force, an indication of joint quality and strength, was measured by tensile-shear testing with a Quad Romulus IV universal mechanical strength tester at a crosshead speed of 90 μm/s (Fig. 1). At least three joints were tested for each run to average the joint breaking force.

In order to observe the interfacial microstructure, the joints were embedded into epoxy resin, sectioned and polished. The microstructure and composition of cross-section of joints were examined using optical microscope (OM) and scanning electron microscope (SEM) with which an energy dispersive X-ray (EDX) spectroscopy is equipped.

Table 1 Chemical composition of 316L stainless steel (wt.%)

C	Mn	Si	Cr	Ni	Mo	S	P	Fe
0.03	2.0	0.75	18	14	2.0	0.03	0.04	Bal

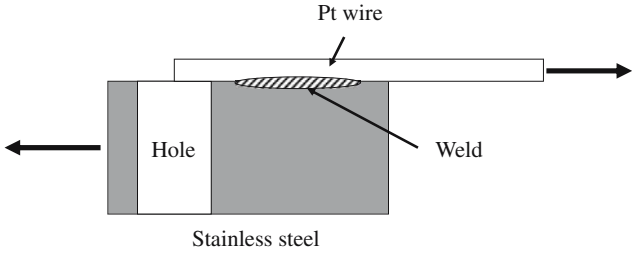

Fig. 1 Schematic illustration of a stainless steel-to-Pt wire joint and measuring breaking force by tensile-shear testing

Results

Effects of welding current and hold time on fusion of materials

Figure 2 shows the SEM top images of resistance micro-welded 316 stainless steel-to-Pt wire joints made at welding currents of 500 A, 750 A and 1,000 A for hold time of 2 ms and 50 ms. It can be clearly seen that at a low welding current of 500 A, no visible melting of either stainless steel or Pt wire during welding could be observed, even though a relative longer hold time (50 ms) had been employed (Fig. 2(a1) and (b1)). When welding current was increased to 750 A, a small fusion of materials was produced at the facing surface with a hold time of 2 ms (as shown by arrow in Fig. 2(a2)). When prolonging the hold time to 50 ms, significant melting of materials which had been squeezed out of the interfacial zone, primarily the stainless steel, was observed, as shown in Fig. 2(b2). However, under this condition, the molten alloy could not well wet the surface of either the stainless steel or the Pt wire, as evidenced by the formation of large solidified alloy balls around the Pt wire (as indicated by arrows in Fig. 2(b2)), probably due to insufficient heat input resulting in a relatively low temperature and hence a poor wettability. On the contrary, a welding current of 1,000 A with only 2 ms hold time resulted in the melting of materials at interface, and particularly the molten alloy well wetted the Pt wire to form a smooth joint (Fig. 2(a3, b3)).

Microstructure of joint interface

SEM low magnification and high magnification cross-sectional images at the bond interface of the joints made at 500 A with various hold times are illustrated in Fig. 3. It can be seen from the low magnification images (Fig. 3(a1)–(a4)) that bonded area increased with increasing hold time. Again it was found that there was no visible interfacial melting in the joints

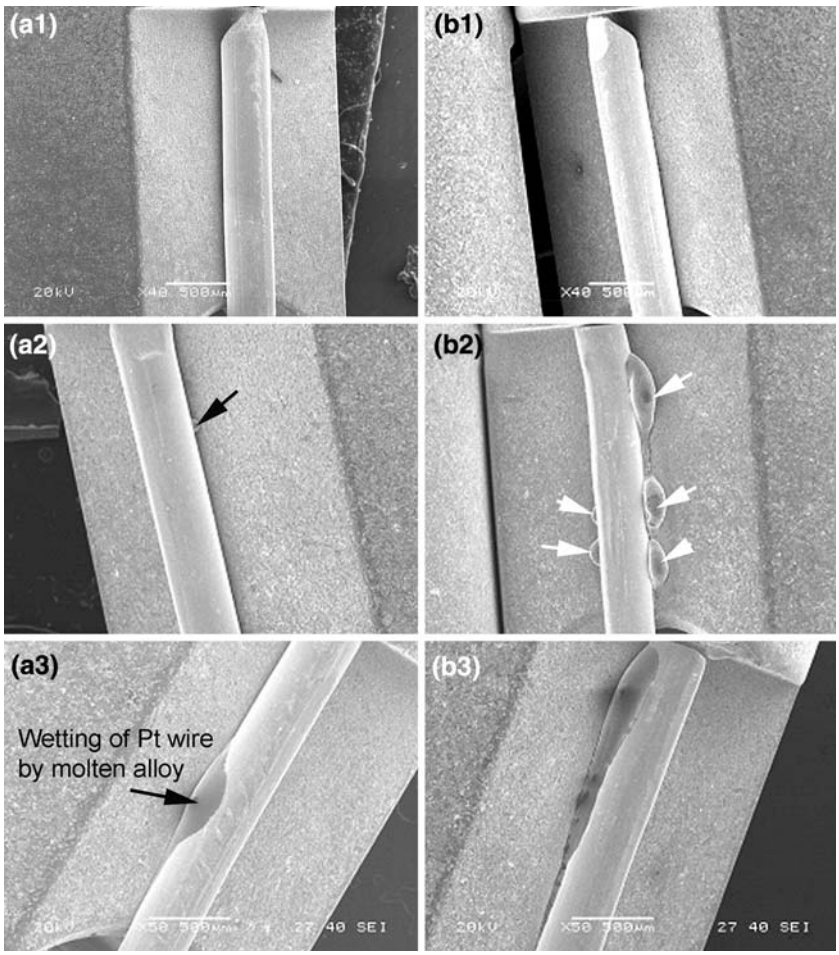

Fig. 2 SEM top images of joints made at 500 A (**a1**, **b1**), 750 A (**a2**, **b2**) and 1,000 A (**a3**, **b3**) for hold time of 2 ms (**a**) and 50 ms (**b**)

welded for 2 ms and 10 ms (Fig. 3(b1) and (b2)), indicating the Pt wire was predominantly bonded to the stainless steel by a solid-state bonding process. With a short hold time of 2 ms, the Pt wire was only locally bonded to the stainless steel as shown by arrows in Fig. 3(b1), and the gap between the Pt wire and stainless steel still existed due to the surface roughness. Increasing hold time to 10 ms produced a relative dense solid-state bonded interface with increased bond area, but a few defects (unbonded or lack of bonding) were still of presence at the interface (Fig. 3(b2)). The melting of materials at interface, primarily stainless steel, occurred when welding with a hold time of 50 ms or more (Fig. 3(a3, b3)). Due to the action of welding force, most of the molten alloy formed at the interface were squeezed out of the interfacial zone to form a 'fillet' (Fig. 3(a3, a4)). When melting at the interface occurred, a dense interface was formed by a process similar to a brazing process (Fig. 3(b3)). However, some voids adjacent to the interface were observed in the region where molten alloy has been solidified (Fig. 3(b4)), indicating the fluidity of molten alloy was still relatively poor.

EDX analysis was carried out to investigate the microstructure and composition of the molten alloy, which has largely been squeezed out of the interfacial zone. Figure 4 shows the more detailed SEM images of the central and edge regions of the joint welded at 500 A for 50 ms (Fig. 3(b3)). The EDX analysis results of regions A–F in Fig. 4 are listed in Table 2. The solidified molten alloy in the edge of the interface (regions A and F) clearly demonstrated a solidification microstructure. It was worth noting that there were mainly two kinds of phases, i.e., Fe-rich phase (regions A, C, D and F) and Pt-rich phase (regions B and E). The Pt-rich phase was only observed at the edge regions as indicated by areas B in Fig. 4(a) and E in Fig. 4(c). As a result, the amount of Pt-rich phase was much less than that of Fe-rich phase, which demonstrated that the molten alloy primarily consisted of the stainless steel. Moreover, based upon the EDX analysis results that the Fe content decreased progressively on going from the alloy squeezed out (region F in Fig. 4(c)) towards the edge of the joint bond interface region (region D Fig. 4(c)), it is deduced that melting of the stainless steel occurred first followed by

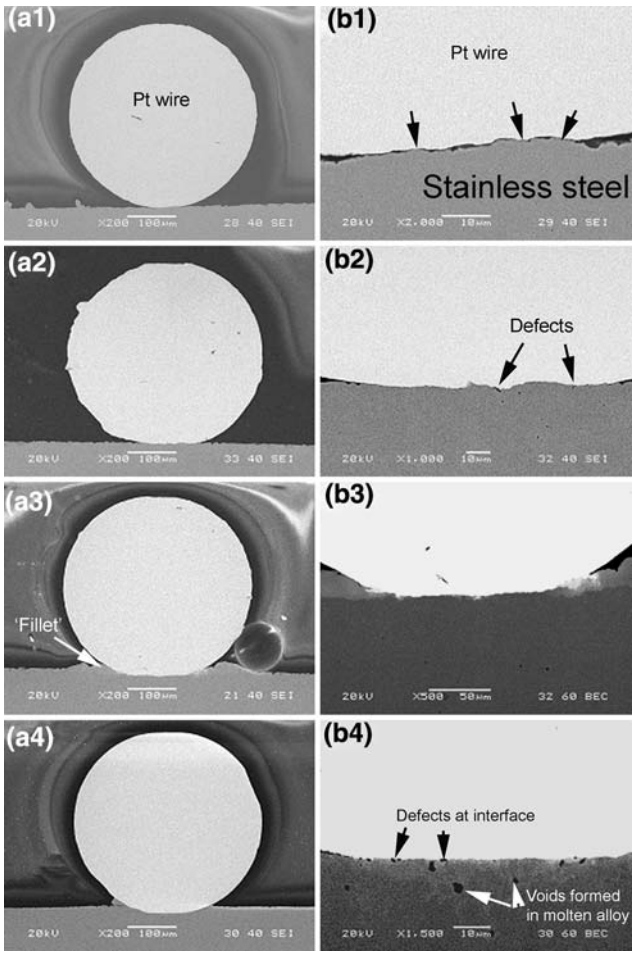

Fig. 3 SEM cross-sectional images of joints made at 500 A with hold times of 2 ms (**a1**, **b1**), 10 ms (**a2**, **b2**), 50 ms (**a3**, **b3**) and 100 ms (**a4**, **b4**). (**b1–b4** show detailed center interfacial regions in (**a1**)–(**a4**), respectively)

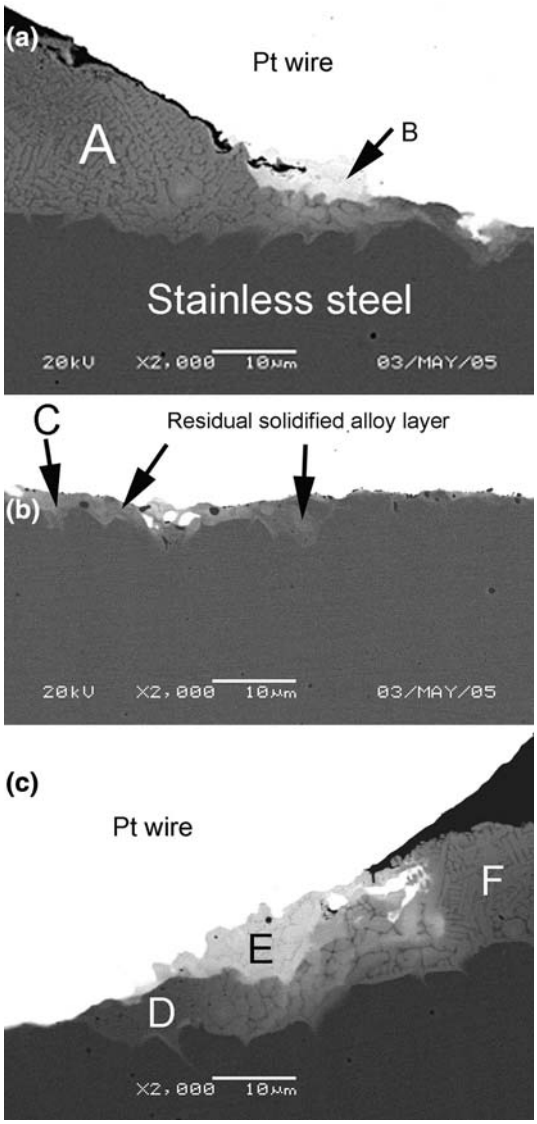

Fig. 4 Detailed SEM images of joint welded at 500 A for 50 ms showing (**a**) left edge region, (**b**) central and (**c**) right edge region (the composition of different regions is listed in Table 2)

Table 2 EDX analysis results of regions A–F in Fig. 4, wt.%

Region	Pt	Fe	Cr	Ni	
A	14.8	59.4	15.9	9.9	Fe-rich
B	70.3	29.7	6.2	3.8	Pt-rich
C	19.7	58.0	13.8	8.6	Fe-rich
D	37.1	44.9	12.6	5.4	Fe-rich
E	57.9	30.1	7.9	4.1	Pt-rich
F	19.5	60.0	13.9	7.6	Fe-rich

subsequent melting or dissolution of the Pt wire substrate adjacent to the interface which then mixed with the molten stainless steel to form a Fe–Pt–Cr–Ni alloy layer. On the other hand, a residual solidified alloy layer was observed between the Pt wire and the stainless steel in the central interfacial region, which showed a similar composition of regions A and F.

As shown in Fig. 5, when welding at 750 A for 2 ms, the bond area between the stainless steel and the Pt wire was much larger than that in the joint made at 500 A for 2 ms (Fig. 4(a1)), indicating temperature rising owing to higher welding current. As a result, the Pt wire plastically deformed in the area adjacent to the interface where temperature was higher due to the contact resistance, even with a short hold time (Fig. 5(a1)). Similar to welding at 500 A, although the Pt wire was also bonded to stainless steel via a solid-state bonding process at 750 A with 2 ms hold time because of no visible melting at the interface, the interface was significantly denser than the former (Fig. 5(b1)). With 10 ms hold time at 750 A (Fig. 5(a2)), a slight melting of materials at the interface was found into which Pt diffused to form a dense

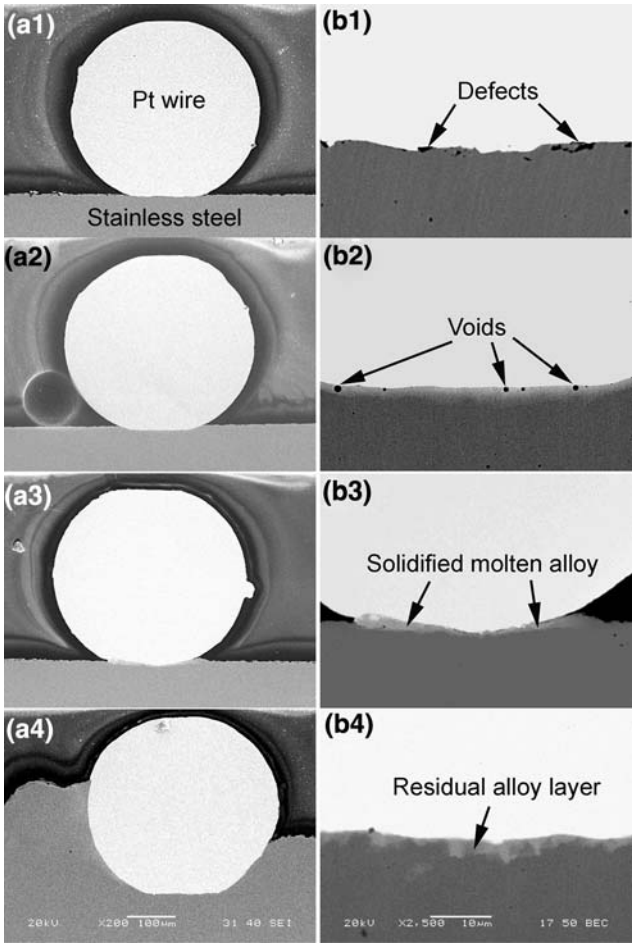

Fig. 5 SEM cross-sectional images joints made at 750 A with hold times of 2 ms (**a1**, **b1**) 10 ms (**a2**, **b2**), 50 ms (**a3**, **b3**) and 100 ms (**a4**, **b4**). (**b1**–**b4** show detailed interfacial regions in (**a1**)–(**a4**), respectively)

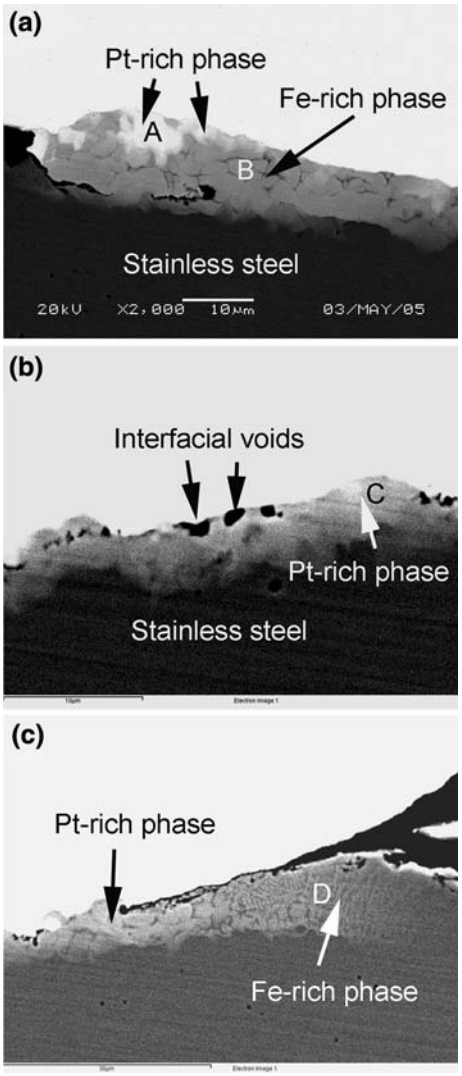

Fig. 6 Detailed SEM images of joint welded at 750 A for 50 ms showing (**a**) left edge region, (**b**) central and (**c**) right edge region (the composition of different regions is listed in Table 3)

interface with a few round solidification voids formed within the fusion zone (Fig. 5(b2)). 50 ms hold time caused more materials melting at the interface where the molten alloy has been squeezed out to the edge of the interface (Fig. 5(a3, b3)). With extremely long hold time (100 ms), the stainless steel was significantly melted and soften adjacent the bond interface, consequently, Pt wire deeply penetrated into the stainless steel to form a very large bond area (Fig. 5(a4)). A residual solidified alloy layer was also observed at the central interfacial region (Fig. 5(b4)). This indicated not all the molten alloy could be squeezed out of interface due to the joint geometry and rapid solidification of molten alloy. However, compared with the joint made at 500 A with 100 ms hold time (Fig. 3(b4)), improved wettability of both stainless steel and Pt wire by molten alloy resulted in a significantly dense interface without interfacial defects at 750 A (Fig. 5(b4)).

The detailed microstructures at the edge and central regions in the joint made at 750 A for 50 ms, as shown in Fig. 6, were very similar to those in the joint welded at 500 A for hold time 50 ms (Fig. 4). The Pt-rich phase and Fe-rich phases were also observed according to the EDX analysis results which were listed in Table 3. However, compared to Fig. 4 and Table 2 (welding current 500 A), it was found that 750 A welding current resulted in more melting of Pt wire and hence both the Pt-rich phase and the Fe-rich phase contained more Pt.

When welding was carried out at 1,000 A, on the other hand, the stainless steel was significantly melted and wetted Pt wire at very earlier stage of welding (2 ms) to form a smooth edge which is similar to the

Table 3 EDX analysis results of regions A–D in Fig. 6, wt.%

Region	Pt	Fe	Cr	Ni	
A	85.0	10.4	3.1	1.6	Pt-rich
B	39.0	41.1	11.7	8.2	Fe-rich
C	47.6	35.7	10.3	6.5	Pt-rich
D	20.7	54.1	15.9	8.9	Fe-rich

'fillet' formed in a brazed joint (Fig. 7(a1)). Prolonging hold time to 10 ms, Pt wire penetrated into stainless steel and more molten alloy was squeezed out to form a large 'fillet' (Fig. 7(a2)).

Joint breaking force and failure mode

The variations of the breaking force of joints as a function of the hold time at welding current of 500 A, 750 A and 1,000 A are summarized in Fig. 8. It was seen that the joint breaking force remarkably increased with the hold time in the initial stage with the hold time less than 10 ms as welding at 500 A and 750 A, owing to the increase in bond area and in interfacial strength due to decrease in interfacial defects and voids. When the hold time longer than 10 ms, those joints maintained a relatively stable breaking force around 4.8 kg. The joints welded at 500 A always showed an interfacial failure mode (Figs. 9, 10). On contrast, the joints made at 750 A showed different failure modes depending on the hold time, i.e., interfacial failure, fractured from interface and then propagated into the Pt wire as well as fractured completely in the Pt wire (Fig. 11). On the other hand, a very short hold time, e.g., 2 ms, was sufficient to form a strong joint (4.8 kg) at 1,000 A which fractured in the Pt wire during loading. At 1,000 A, although increasing the hold time to 10 ms could give small increase in breaking force, eventually the breaking force was decreased due to welding heat induced softening of Pt wire (hardness decreased from HV 155 before welding to HV 140 after welding at 1,000 A for 50 ms). Therefore, the welding process needs sufficient heat to form joint and improve the strength (from solid-state bonding to fusion (or brazing)), but too high a heat will degrade Pt wire.

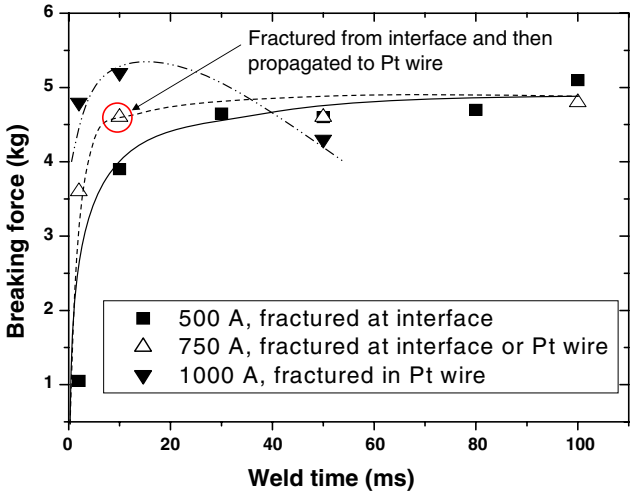

Fig. 8 Dependence of breaking force of joints on hold time at welding current of 500 A, 750 A and 1,000 A

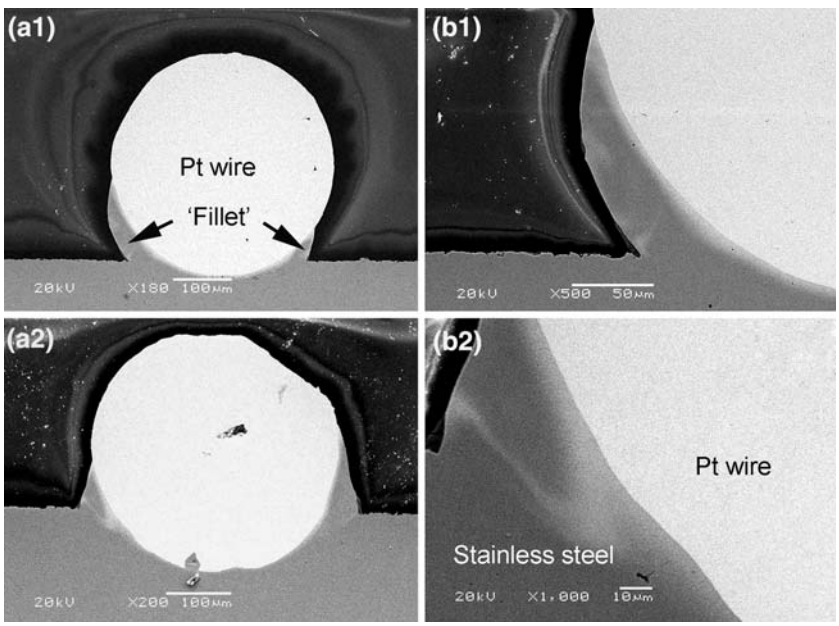

Fig. 7 SEM cross-sectional images of joints made at 1,000 A with hold times of 2 ms (**a1**, **b1**) and 10 ms (**a2**, **b2**). (**b1**–**b2** show detailed center interfacial regions in (**a1**)–(**a2**), respectively)

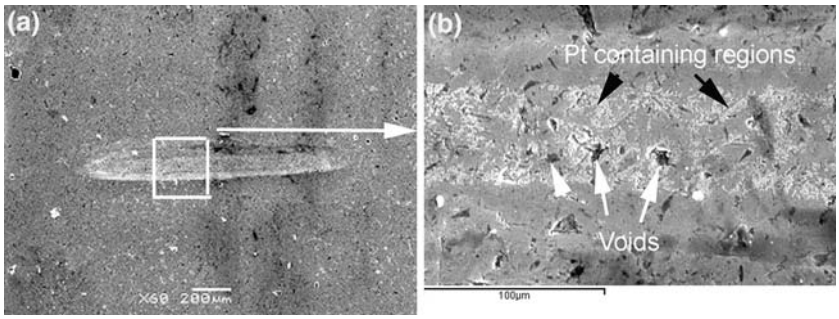

Fig. 9 SEM fractured stainless steel surface of joint made at welding current of 500 A with 10 ms hold time after tensile-shear testing showing (**a**) low magnification image and (**b**) detailed structure of square region in (**a**)

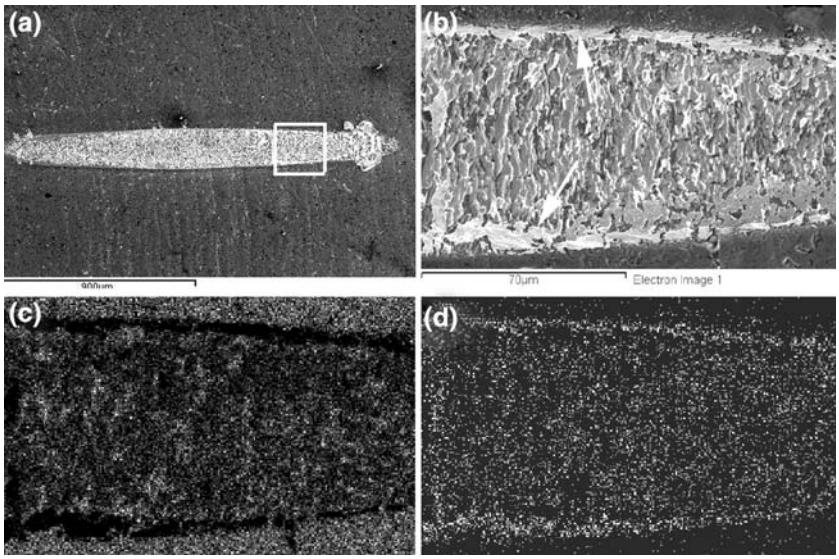

Fig. 10 SEM fractured stainless steel surface of joint made at welding current of 500 A with 50 ms hold time after tensile-shear testing showing (**a**) low magnification image, (**b**) detailed structure of square region in (**a**), (**c**) FeK_{α} and (**d**) PtK_{α} corresponding to (**b**)

After measurement of the joint breaking force, the fracture surfaces of the specimens were examined using SEM and EDX in order to clarify the fracture mechanisms. Figures 9 and 10 illustrate the stainless steel surface of two joints made at welding current of 500 A after tensile-shear testing. It clearly showed that the Pt wire has been peeled off from the stainless steel, i.e., fracture at the interface, leaving a mark which indicated the bonded area between the Pt wire and the stainless steel. Consistence with cross-section view (Fig. 3) which showed an increase of bond area in transverse direction, Figs. 9 and 10 demonstrated that bond area of joints increased with increasing hold time also in the longitudinal direction. Some interfacial defects (lack of bonding and/or voids) could be observed on the fractured surface with a short hold time (10 ms) which resulted in a solid state bond interface (Fig. 9(b)). EDX analyses revealed that the shallow gray areas in the middle region contained Pt, as indicated by black arrows on the fracture surface (Fig. 9(b)). This demonstrated the interdiffusion or adhesion between the Pt and the stainless steel has occurred, which resulted in local fracture within alloyed layer or in the Pt wire at strongly bonded regions. When materials melting at the interface occurred, dendritic solidified microstructure could be seen on the fractured surface (Fig. 10). In addition, it was interesting to note that there were Pt-rich regions at the edge of bonded interface (as shown by arrows), which was quite consistent with the observations of cross-section where the Pt-rich phase was also observed at the edge of the interface (Figs. 3, 5). On the other hand, Fig. 11 shows interfacial failure (Fig. 11(a)), fracture initiation at the interface and then propagation into Pt wire (Fig. 11(b)) as well as completely fracture in the Pt wire (Fig. 11(c)) of the joint welded at 750 A with different hold time. The fracture of all the joints made at 1,000 A was similar to those at 750 A with hold time longer than 50 ms.

The alloy layer containing Fe, Pt, Cr and Ni formed at the interface especially with melting of materials probably contains binary or ternary intermetallic compounds according to Fe–Pt and Cr–Pt phase diagrams [14]. Usually the formation of intermetallic compounds would be harmful for interfacial strength

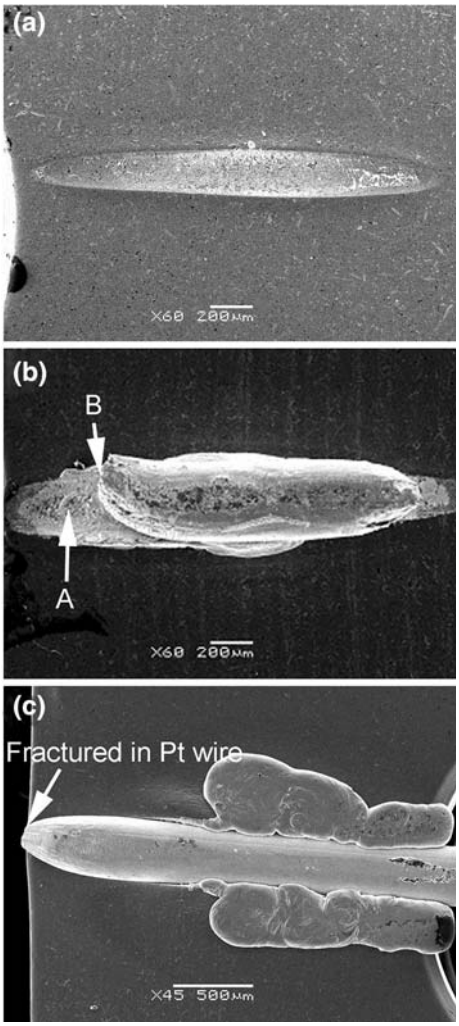

Fig. 11 SEM images of fractured joints welded at 750 A with hold time of 2 ms (**a**), 10 ms (**b**) and 100 ms (**c**)

and hence causes fracture at interface. However, the interfacial alloy layer seems no much effect on joint failure and strength in this work, as evidenced by fracture in Pt wire (not interface) as materials melting to form a alloy layer at relative high welding current.

Discussion

The experimental results demonstrated that either the solid-state bonding without fusion of either the stainless steel or the Pt wire or the fusion welding with melting of materials at the interface occurred depending on the welding current and/or hold time (heat generation). In the case of bonding with fusion, the melted materials, primarily the stainless steel, were squeezed out of interfacial zone due the joint configuration. It is known that heat generation in resistance welding can be expressed as follows [15],

$$Q_{\mathrm{G}} = I^2Rt \tag{1}$$

where, I is the welding current, R is the electrical resistance of the workpiece, and t is the weld time (hold time). Therefore, the heat generation is determined by both process parameters (i.e., welding current and weld time), and the electrical resistivity and geometrical shape of the workpiece. The heat generated from the electrodes is neglected in the analysis, which is a good approximation since the electrical resistivity of Class 2 electrodes is very low. The heat generated from the contact resistance at facing interfaces is also neglected to keep the analysis simple and workable, which may be reasonable when Pt wire was brought into intimate contact with stainless steel by plastic deformation after a short time of welding, for example, a few seconds.

Joint formation depends on the interplay of heat generation (Q_{G}) and heat dissipation (Q_{D}) which is determined by the thermal conductivities and geometrical shapes of the workpiece and electrodes in the electrode-workpiece system, i.e., [16],

$$Q_{\mathrm{G}} = Q_{\mathrm{J}} + Q_{\mathrm{D}} \tag{2}$$

where, Q_{J} is the total heat required to form a joint. Assuming $Q_{\mathrm{D}} = fQ_{\mathrm{G}}$, then Eq. 2 becomes,

$$Q_{\mathrm{G}} = Q_{\mathrm{J}}/(1-f) \tag{3}$$

where, f is a ratio determined by the relative magnitude of Q_{D} and Q_{G}.

The total heat (Q_{SJ}), required to form a solid-state bonded joint, needs to heat one of the materials which has a lower melting point, i.e., stainless steel in this work, to a high temperature of 0.7–0.8 T_{m} (T_{m}, melting point) to ensure plastic deformation and diffusion occur. On the contrary, in order to form a joint with fusion of materials at the interface, the total heat (Q_{FJ}) should be high enough to heat the material to its melting point and melt it. Therefore, Q_{FJ} can be expressed as,

$$Q_{\mathrm{FJ}} = q_{\mathrm{FJ}}V = (\rho C_p \Delta T + \rho H)V \tag{4}$$

where, q_{FJ} is the total heat to form a fusion joint per unit volume, ρ is the density of material, C_p is the specific heat, ΔT is the temperature rise from room temperature to the melting point, V is the volume of melted material, and H is the latent heat of fusion per unit volume. Combining Eqs. (1)–(4) leads to,

$$I^2 t = \frac{q_{FJ} V}{R(1-f)} \tag{5}$$

By considering two kinds of joints made of individual material, i.e., stainless steel-to-stainless steel and Pt-to-Pt, we may compare the welding current required to produce a certain volume fusion at an identical weld time for different materials. The above equation can be arranged to be,

$$I_{SS} : I_{Pt} = \left(\sqrt{\frac{q_{FJ}}{(1-f)R}}\right)_{SS} : \left(\sqrt{\frac{q_{FJ}}{(1-f)R}}\right)_{Pt} \tag{6}$$

If we assume that the geometry of the stainless steel and the Pt as well as the f value were identical, the resistivity of materials can be used to replace R in Eq. 6 and the term (1 – f) can be canceled out from Eq. 6. As a result, the welding current values in Eq. 6 are calculated using material's resistivity and q_{FJ} (Table 4) and then normalized using the calculated current for stainless steel:

$$I_{SS} : I_{Pt} = 1 : 6.8 \tag{7}$$

This means that the welding current for making melting of Pt is about seven times higher than that for melting stainless steel. Consequently, when welding stainless steel to Pt, the stainless steel will first be melted as welding current increases, whereas Pt still maintains solid state without melting. This phenomena has been observed in the experiments (Figs. 2–6).

At a relative higher welding current, both the stainless steel and the Pt could be melted during welding. Using above assumptions, we can arrange Eq. 5 to obtain the ratio of volume of melted stainless steel to that of melted Pt as follows,

$$V_{SSM} : V_{PtM} = \left(\frac{R}{q_{FJ}}\right)_{SS} : \left(\frac{R}{q_{FJ}}\right)_{Pt} = 6.8 : 1 \tag{8}$$

Table 4 Physical properties used for calculations of total heat (q_{FJ}) by Eq. 4

	316L stainless steel	Pt
Melting point (°C)	1,420	1,772
ΔT (K)	1,668	2,020
Thermal conductivity (W/m/K)	16.3	73
Electrical resistivity ($\mu\Omega$ cm)	74	9.85
Density (g/cm^3)	8	21.5
Specific heat at 20 °C (J/kg/K)	500	130
Latent heat of fusion (J/g)	247	101
Total heat (q_{FJ}) by Eq. 4	117	792

It is contrary to the ratio of welding current required to melt stainless steel and Pt, Eq. 8 demonstrates that at a fixed welding current and weld time, the volume of melted stainless steel is around seven times more than that of melted Pt. Similarly, this phenomenon has also been observed in the experiments (Figs. 4, 6). In addition, less thermal conductivity of stainless steel favors to keep it at high temperature for longer time, and hence promoting its melting. The model proposed here can also be employed to analyses and predict the resistance welding process of dissimilar materials due to their different physical properties.

On the other hand, due to melting of Pt requires much high welding current compared to stainless steel, consequently, only very small amount of Pt-rich phase resulting from melting was mainly observed at the edge region of the joint interface (Fig. 4) where the current density is largest due to the joint configuration.

Conclusion

The Interfacial metallurgical phenomena and mechanical property of micro-resistance welded 316L stainless steel-to-Pt wire joints were investigated. The following are some of the major conclusions.

1. The mechanism of joint formation during RMW of 316L stainless steel-to-Pt wire involves solid-state bonding at low welding current and/or short weld time as well as a fusion welding at high welding current and/or long weld time.
2. The joint breaking force increases with increasing welding current and weld time in the initial stage of welding due to increased bonded area and interfacial bonding strength.
3. The joints welded at low welding current usually correspond to an interfacial failure; whereas the joints made at high welding current fracture within the Pt wire.
4. The amount of melted stainless steel is significantly larger than that of Pt wire due to their different physical properties. As a result, only a small amount of Pt-rich phase resulting from melting of the Pt wire was observed at the edge region of the joint interface.

References

1. Sudhakar KV (2005) Eng Failure Anal 12:249
2. Keun-Taek Oh, Young-Sik Kim, Yong-Soo Park, Kyoung-Nam Kim (2004) J Biomed Mater Res 69B:183

3. Haynes DR, Crotti TN, Haywood MR (2000) J Biomed Mater Res 49:167
4. Baba N, Watanabe I, Liu J, Atsuta M (2004) J Biomed Mater Res 69B:121
5. Noolua NJ, Kerr HW, Zhou Y, Xie J (2005) Mater Sci Eng A 397:8–15
6. Ferrante M, Pigoretti EV (2002) J Mater Sci 37:2825, Doi: 10.1023/A:1015845822629
7. Johson KI (1985) Introduction to microjoining. TWI, Abington, United Kingdom
8. Tan W, Zhou Y, Kerr HW (2002) Metall Mater Trans A 33A:2667
9. Fukomoto S, Zhou Y Metall (2004) Metall Mater Trans A 35A:3165
10. Fukomoto S, Chen Z, Zhou Y (2005) Metall Mater Trans A 36A:2717
11. Dong SJ, Zhou Y (2003) Metall Mater Trans A 34A:1501
12. Dong SJ, Kelkar GP, Zhou Y (2002) IEEE Trans Electron Packag Manufact 25:355
13. Zhou Y, Dong SJ, Ely KJ (2001) J Electron Mater 30:1012
14. Massalski TB (1990) Binary alloy phase diagrams. ASM International, Materials Park, OH
15. Resistance Welder Manufactures' Association (RWMA) (1989) Resistance welding manual, 4th edn, George H. Buchanan Co., Philadelphia, Sect 1
16. Zhou Y, Gorman P, Tan W, Ely KJ (2000) J Electron Mater 29:1090